Optical properties of a silver-related defect in silicon

Davies, G.; Gregorkiewicz, T.; Zafar Iqbal, M.; Kleverman, M.; Lightowlers, E.C.; Vinh, N.Q.; Zhu, M.

Publication date
2003

Published in
Physical Review B

Optical properties of a silver-related defect in silicon

Gordon Davies,[1] T. Gregorkiewicz,[2] M. Zafar Iqbal,[1,3] M. Kleverman,[4] E. C. Lightowlers[1,*] N. Q. Vinh,[2] and Mengxia Zhu[1]
[1]*Department of Physics, King's College London, Strand, London WC2R 2LS, United Kingdom*
[2]*Van der Waals-Zeeman Institute, University of Amsterdam, Valckenierstraat 65, NL-1018 XE Amsterdam, The Netherlands*
[3]*Department of Physics, Quaid-I-Azam University, Islamabad 45320, Pakistan*
[4]*Solid State Physics, Lund University, Box 118, S-221 00, Sweden*
(Received 5 December 2002; published 27 June 2003)

Doping crystalline silicon with silver results in a photoluminescence center with multiplet zero-phonon structure near 778.9 meV. We show that the published assignments of the vibronic sidebands are wrong, with severe implications for the relative transition probabilities of the luminescence transitions from the excited states. At low temperature, most of the luminescence intensity derives from the phonon sideband associated with a *forbidden* zero-phonon line through the phonon-assisted coupling of two of the excited states of the center. The effective mass of the vibration is determined from isotope effects to be close to the mass of one Ag atom. Uniaxial stress and magnetic perturbations establish that the current assignment of the electronic structure of the center is incorrect and that it is best described by a new variant on the ''pseudodonor'' model. An electron orbits in an effective T_d environment, with an orbital *triplet* as its lowest-energy state, giving a $j=3/2$ electron state. A tightly bound hole has its orbital angular momentum quenched by the C_{3v} symmetry of the center, leaving only spin angular momentum ($s=1/2$). These particles couple to give $J=2,1,0$ states. Using this model, the temperature dependence of both the total luminescence intensity and measured radiative decay time can be understood. These data allow an estimate to be made of the thermally induced transition rate of the electron from the effective-mass excited states into the conduction band.

DOI: 10.1103/PhysRevB.67.235111 PACS number(s): 71.55.Cn, 78.30.Am

I. INTRODUCTION

It is well established that the photoluminescence of many optical centers in crystalline silicon can be described in terms of the recombination of an electron and a hole at an electrically neutral center. Usually, one of these particles is tightly bound and the other is loosely bound. With increasing temperature, the luminescence from the centers is always quenched. However, within this generic model there is considerable diversity. The activation energy for the luminescence quenching may be equal to the binding energy of the loosely bound particle (e.g., the well-known 1014-meV Cu-related luminescence[1]), that of the tightly bound particle (e.g., the 968-meV Cu-S center[2]), that of the binding energy of the exciton to the center (e.g., the *I*2 boron-related center[3]), or it may equal the binding energy of the free exciton (e.g., the *W* center[4]). The tightly bound particle may be the electron, with the loosely bound hole maintaining its orbital angular momentum, but being split into a doublet of nearly equal transition strengths (e.g., the 935-meV C-related center[5]). Alternatively, the hole may be tightly bound, quenching its orbital angular momentum and leading to spin-triplet, spin-singlet states (e.g., the *Q* Li-related center[6]) with a doublet zero-phonon structure of one almost forbidden line and one allowed transition. The relative strengths of transitions from these ''triplet'' and ''singlet'' states can be predicted simply from the effect on the valence-band maxima of the field binding the hole.[7] In all these cases the lowest-energy electron state is an A_1 state derived from the conduction-band minima.

Many centers can be produced by doping crystalline silicon with silver, as shown by Refs. 8–11 and the work cited therein. In this paper we examine the multiple-excited state structure of one center. We will show that it can be described by using another variant on the bound-exciton model. The lowest-energy states consist of an effective-mass electron in a *triply degenerate* orbital state and a tightly bound hole. The response of the electron to external perturbations is determined by its effective T_d environment, while the response of the hole is that of a nondegenerate orbital state at a center of trigonal symmetry. The low-symmetry environment of the hole quenches its orbital angular momentum, and spin-spin coupling dominates in the interaction of the electron and hole. We will show that these states interact so as to produce a very unusual vibronic structure and that the changes in luminescence intensity of the band, as functions of both temperature and secondary excitation, can be understood using the model for the electronic states.

The center, which produces the 779-meV-photoluminescence (PL) system, Fig. 1, has been reported frequently.[11–20] Isotope doping has confirmed the presence of Ag in the center.[19] It has been established that the three zero-phonon lines ''*A*'' at 778.9 meV, ''*B*'' at 779.9 meV, and ''*C*'' at 784.4 meV are transitions to the same ground state.[14] The energies of the transitions establish[10] that they occur at the same center that produces the E_v+340 meV deep-level transient spectroscopy (DLTS) signal.[8] From the Fano structure of the ionization continuum of the center, it was deduced that the transitions occurred at a deep donor,[11] later refined to be a ''pseudodonor'' (i.e., an electrically neutral center where an effective-mass electron can orbit in the Coulomb field of a tightly bound hole).[13] The effective-mass electron state, derived from the six conduction-band minima, is expected to split into A_1, E, and T_2 states (Sec. IV) and the excited state of the *C* line has been ascribed to the A_1 state.[12,13] Splittings in the transitions assigned to the E and T_2 states have led to

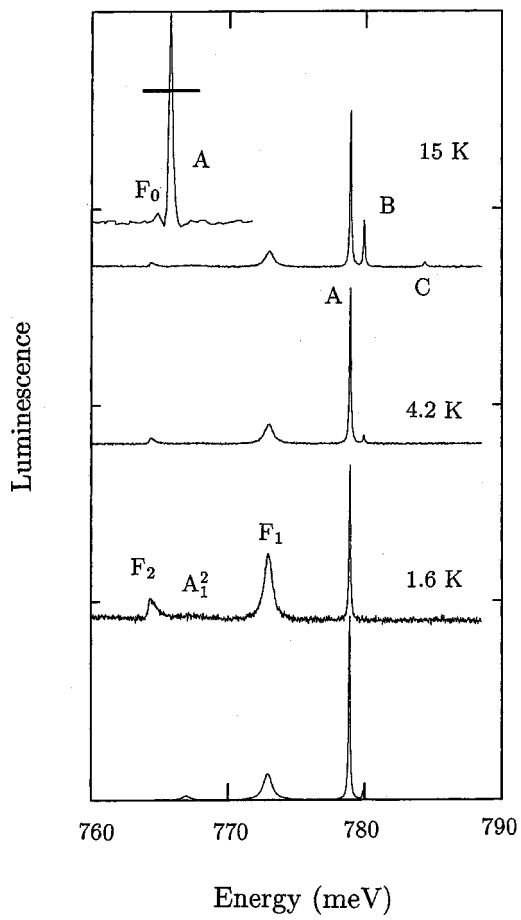

FIG. 1. The upper three spectra show measured photoluminescence spectra of the 779-meV center in silicon at 1.6, 4.2, and 15 K. Two one-phonon resonance modes, labeled F_1 and F_2, are observed. The zero-phonon line A weakens relative to F_1 and F_2 on cooling from 4.2 to 1.6 K. The inset at the top shows an enlarged (and shifted) spectrum of the A and F_0 lines at 1.6 K. The marker is 1 meV long. The lowest curve shows the luminescence spectrum calculated as in Sec. V and for 4.2 K. The peaks are simulated using Lorentzian line shapes with the widths as determined from experiment and the intensities calculated with the parameters that give the best fit to the energy levels. In the calculation, only the F_1 mode has been considered. The F_2 mode would be produced by the same process as for F_1.

the suggestion that the symmetry of the center is C_{2v}.[11] The symmetry has also been assigned to T_d on the basis of a possible link to the NL42 paramagnetic resonance center.[15] The phonon replicas are stated to be phonon sidebands of the *A*, *B*, and *C* zero-phonon lines.[14] However, despite the many publications, there has been no unified description of the optical properties of the center including the observed responses to external perturbations.

We show in this paper that the assignments of the vibronic sidebands are wrong, with severe implications for the relative transition probabilities of the luminescence transitions from the excited states. At low temperature, most of the PL intensity derives from the phonon sideband associated with a *forbidden* zero-phonon line (Sec. III). The responses of the excited states to uniaxial stress and magnetic field perturbations are presented in Sec. IV. The large splitting of line *C* under uniaxial stress establishes that the excited state should be assigned to a T_2 effective-mass orbital state in T_d symmetry, rather than the current assignment to an A_1 orbital. We show that the low-symmetry environment of the hole quenches its orbital angular momentum and spin-spin coupling dominates in the interaction of the electron and hole. The mechanism through which the vibronic sideband is produced is presented in Sec. V, and by using isotope data to estimate the effective mass of the vibration, it is shown to be consistent with the perturbation data (Sec. VI). Knowing the electronic structure, the temperature dependence of both the total PL intensity and the measured radiative decay time can be understood, and we make a first estimate of the transition rate for thermal quenching of a ''pseudodonor'' in silicon. (Sec. VII). We begin by presenting the experimental method and preparation of the samples.

II. SAMPLE PREPARATION AND EXPERIMENTAL METHOD

The center was produced from relatively pure float-zone silicon, including 1000 Ω cm *n* type, with an oxygen concentration $[O]<10^{14}$ cm^{-3} and carbon $[C]\sim 5\times 10^{15}$ cm^{-3}, and 100 Ω cm *p* type. The material was first gettered to drive out Cu atoms. It was then HF/HNO_3 etched, RCA cleaned, and HF dipped before Ag was evaporated on one side. The slices were heated at 1100–1150 °C for 4–20 h in a quartz tube in flowing Ar gas, cooled down either in the tube or quenched to room temperature in water, and the surface was etched to remove about 70 μm. Natural and isotopically enriched silver (99.5% ^{107}Ag and 99.4% ^{109}Ag) were used. Optical measurements were carried out using a variety of Fourier transform spectrometers and dispersive spectrometers, fitted with germanium diode detectors. The luminescence spectroscopy was carried out using 514-nm Ar^+ lasers operating at constant powers of typically 400 mW. Uniaxial stress measurements were carried out at temperatures from 4.2 up to 20 K and with stresses up to 200 MPa. For the Zeeman measurements, the magnetic field was varied from 0 up to 4.5 T. Time-resolved measurements were carried out using a Tektronic TDS 3032 digital oscilloscope in combination with a Hamamatsu R5509-72 InP/InGaAs photomultiplier tube. For the lifetime data of Sec. VII, transient excitation was obtained by chopping the laser excitation beam mechanically at 200 Hz. The system response time was measured as 38 μs. For the two-beam experiments, luminescence from the Ag center was excited by a frequency-doubled Nd:YAG laser with pulse lengths of several ns. A free-electron laser, giving pulses of 5–7 μs, was fired with a delay time of up to 1 ms relative to the Nd:YAG pulses. The free-electron laser was tunable in the range 70–170 meV.

III. STRUCTURE OF THE LUMINESCENCE BAND

Usually, as the temperature decreases, the zero-phonon line of a band increases in intensity relative to the vibronic sideband. Figure 1 shows that between 4.2 and 1.6 K the line *A* weakens relative to the phonon sideband. Line *A* is evi-

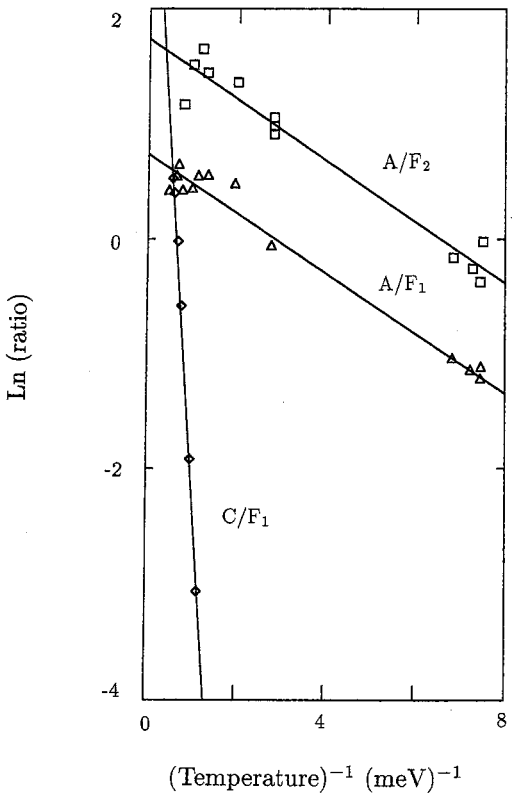

FIG. 2. Arrenhius plots of the variation with temperature of the intensities of line *A* relative to F_1 (triangles), *A* relative to F_2 (squares), and *C* relative to F_1 (diamonds). Both of the activation energies for line *A* are ~0.26 meV, equal to the spectroscopic separation of *A* from the ''forbidden'' line F_0, and the activation energy for line *C* is ~5.8 meV, equal to the spectroscopic splitting of F_0 and *C*.

dently not the zero-phonon line of the low-temperature band, in contrast to the assignments by Refs. 15 and 17. Below 2 K a very weak line F_0 is resolved at 778.6 meV, 0.25 meV below *A*, as shown in the enlarged inset to Fig. 1. The ratios of the phonon sidebands F_1 and F_2 are temperature independent, Fig. 1, demonstrating that they derive from the same initial state. Their associated zero-phonon line is established by the data in Fig. 2, where we show the variations with temperature of the intensity ratios of *A* to F_1 and of *A* to F_2. Both ratios follow Arrhennius behavior, with activation energies, respectively, of 0.26 ± 0.02 and 0.26 ± 0.3 meV, equal to the energy separations of the zero-phonon lines *A* and F_0. The zero-phonon line associated with the sidebands F_1 and F_2 is therefore F_0, not the stronger *A*. Similarly, the ratio of *C* to F_1 has an activation energy of 5.8 ± 0.9 meV, equal to the spectroscopic splitting of F_0 and *C* (5.7 meV). From the data in Fig. 2, the intensity ratio of lines *C* and *A* extrapolated to infinite temperature is $I_C/I_A=21\pm6$, similar to the value of 28 measured directly from the ratio of I_C/I_A by Iqbal *et al.*[14] We also agree with their result that $I_B/I_A=0.7\pm0.05$.

By extrapolating the measured ratios to infinite temperature, the total transition probabilities in the *F* bands (F_1+F_2) relative to *A*, *B*, and *C* are

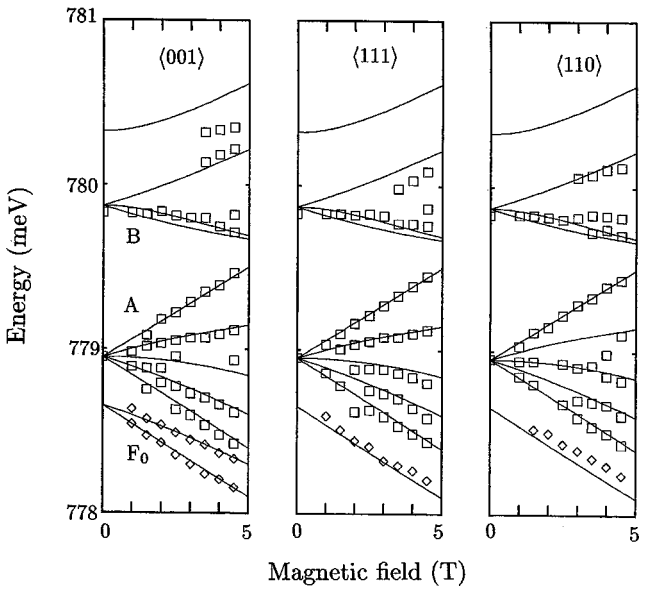

FIG. 3. The squares show the Zeeman effect measured for the zero-phonon lines *A* and *B*, and the diamonds show transitions induced from F_0. Line *C*, which is not shown, does not shift, as expected from the model of Sec. IV. The lines are calculated as in Sec. IV with parameters $\lambda=-0.46$ meV, $g_s=1.9$, and $g_l=0$. The lines close to the data for F_0 have been obtained by downshifting the fits to the lowest-energy components of line *A*.

$$I_F/I_A=0.68\pm0.04, \quad I_F/I_B=1.0\pm0.1,$$

$$I_F/I_C=0.032\pm0.016. \tag{1}$$

The phonon energies of the well-defined sidebands F_1 and F_2, measured from the zero-phonon level F_0, are, respectively, $\hbar\omega_1=5.8$ meV and $\hbar\omega_2=14.6$ meV. The spectra of Fig. 1 show no discernible contributions to the sideband arising from line *B*. Lines *A* and F_0 are sufficiently close that their phonon sidebands would not be separately resolved. To place an upper limit on the strength of coupling of *A* to the 5.8-meV mode, suppose that the *A* transitions contribute a fraction *f* to the phonon sideband F_1, with the remainder arising from F_0. Then the ratio of $I_A/(1-f)I_{F1}$ should obey a Boltzmann ratio with an activation energy equal to the separation of the lines *A* and F_0. Taking account of experimental uncertainties, a maximum of 15% of the transition from level *A* can go to the one-phonon line F_1, so that to a good approximation transition *A* does not couple to *one* quantum of the 5.8-meV mode. The dominant luminescence at low temperature is therefore associated with an essentially forbidden line F_0. The peak at 767.2 meV, labeled A_1^2 in Fig. 1, is assigned to a *two-phonon* assisted transition of the 5.8-meV mode and line *A*. The mechanism producing these vibronic effects is presented in Sec. V.

IV. PERTURBATIONS OF THE ZERO-PHONON LINES BY MAGNETIC AND STRESS FIELDS

The effects of magnetic fields on the lower-energy lines were measured at 4.2 and 20 K by photoluminescence (Fig. 3) and by optical absorption at 4.2 K for the higher-energy

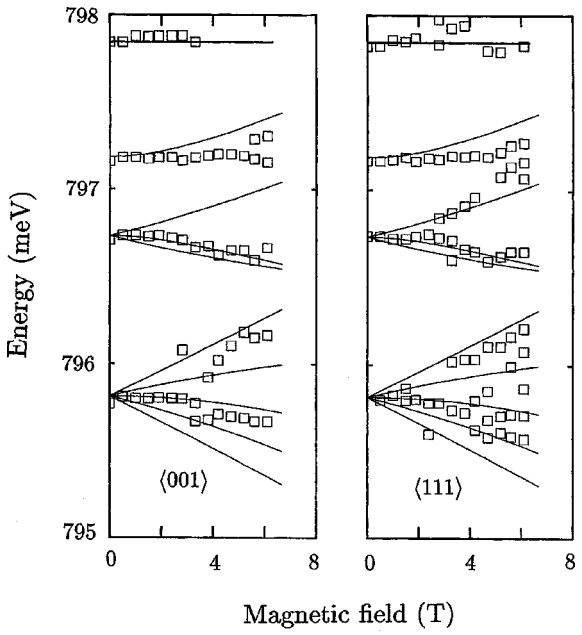

FIG. 4. Zeeman effect of the higher excited states, labeled as $1s(E+T_2)$ in Ref. 9, with the magnetic field along ⟨001⟩ and ⟨111⟩ directions. The squares are the experimental data, and the lines are calculated using the spin-orbit parameter $\lambda=-0.46$ meV derived from the fit of the Zeeman effect on the lines *A* and *B* (Fig. 3) and a spin *g* factor $g_s=1.3$. The line at 797.9 meV is assigned to the transition from the singlet state, analogous to line *C*.

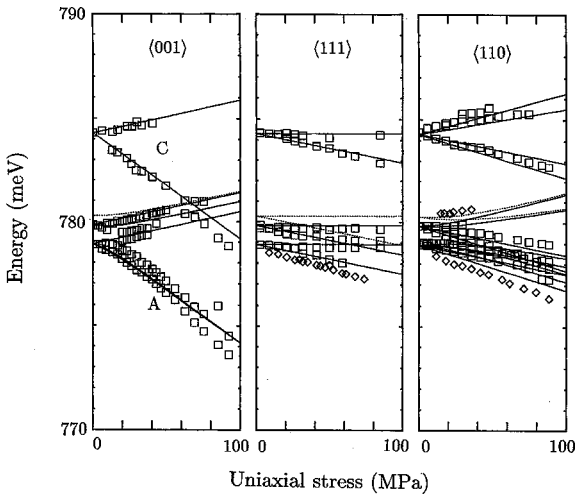

FIG. 5. The squares show the data for the splittings of the zero-phonon lines under stress along the ⟨001⟩, ⟨111⟩, and ⟨110⟩ crystal directions, measured in luminescence at 4.2 and 20 K. Experimental data for the transitions induced by the stresses are shown by diamonds. The lines are the fits derived from the model described in Sec. IV. Dashed lines originating near 780.2 meV show the predicted energies of the $J=0$ state.

transitions near 796 meV (Fig. 4). Line *C* is not affected by the field. The effect of uniaxial stresses are shown for the lower energy lines in Fig. 5, using luminescence at 4.2 and 20 K to enhance these low-energy transitions, and in Fig. 6, using absorption measurements to monitor also the higher energy states.

The magnetic perturbations are isotropic within measuring accuracy and so contain no information about the point group of the center. This result supports the proposal that the hole is tightly bound,[13] because then its orbital angular momentum is quenched, leaving only its spin angular momentum, which responds isotropically to the magnetic field at the resolution available optically.

The effects of stress are most easily seen for line *C* (Figs. 5 and 6). The line splits under ⟨001⟩ stress at the rate of 79 ± 2 meV/GPa, similar to the splitting of the conduction-band minima [92.5 meV/GPa (Ref. 21)], while there is little splitting under ⟨111⟩ stress. These results confirm the effective-mass nature of the electron. The electron state is derived from the six conduction-band minima and so transforms as A_1, E, and T_2 states in T_d symmetry. In a basis set ordered as A_1, E_θ, E_ϵ and T_2^x, T_2^y, T_2^z, these valley orbit states are perturbed under stress according to the symmetric matrix[22]

$$\begin{pmatrix} -\gamma(5+\delta) & ps_\theta & ps_\epsilon & 0 & 0 & 0 \\ & -Bs_\theta+\gamma(1-\delta) & Bs_\epsilon & 0 & 0 & 0 \\ & & Bs_\theta+\gamma(1-\delta) & 0 & 0 & 0 \\ & & & C(\sqrt{3}s_\epsilon-s_\theta) & 0 & 0 \\ & & & & -C(s_\theta+\sqrt{3}s_\epsilon) & 0 \\ & & & & & 2Cs_\theta \end{pmatrix}. \tag{2}$$

Here 6γ is the energy separation of the E state from the A_1 state and $2\delta\gamma$ is the displacement of the T_2 state from E. The terms s_θ and s_ϵ are the stress combinations

$$s_\theta=2s_{zz}-s_{xx}-s_{yy}, \quad s_\epsilon=\sqrt{3}(s_{xx}-s_{yy}),$$

where the stress tensor components s_{ij} are written in terms of the Cartesian coordinates $i,j=x,y,z$ of the crystal and compressive stress is defined to be positive. Hydrostatic stress terms, which would appear down the diagonal of the matrix, are omitted (and will be introduced below).

An A_1 state is perturbed only by hydrostatic stresses and

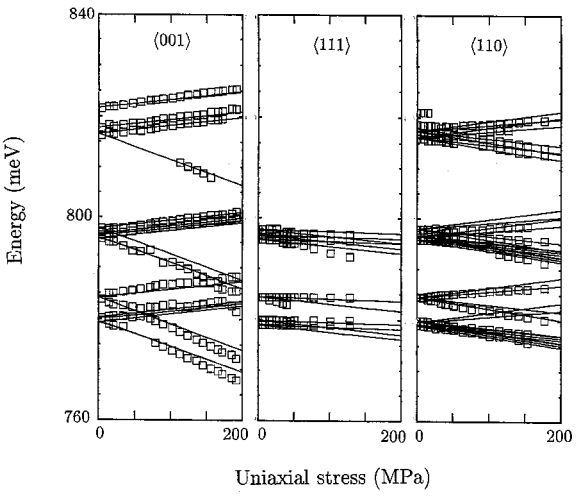

FIG. 6. The squares show the data for the splittings of the zero-phonon lines under stress along the ⟨001⟩, ⟨111⟩, and ⟨110⟩ crystal directions, measured in absorption at 4.2 K. The lines are the fits derived from the model described in Sec. IV.

by coupling through the terms ps_θ and ps_ϵ to the E state, Eq. (2). The considerable splitting of line C under ⟨001⟩ stress and the linearity of the splitting establishes that C does not have an A_1 state, as is central to existing descriptions of the excited states of the center.[11] Line C derives from the T_2 component of Eq. (2).

Under stress, the matrix shows that the T_2 state splits into two components under ⟨110⟩ stress and is not split under ⟨111⟩ stress. Consequently, to obtain the two components seen in ⟨001⟩ stress, two in ⟨111⟩, and at least three in ⟨110⟩ stress, the hole must not be split under ⟨001⟩ stress and must be perturbed into two states by ⟨111⟩ stress and by ⟨110⟩ stress. These splittings are only expected for an orbitally nondegenerate state in a trigonal local symmetry,[23] which defines the environment of the hole.

Having determined the environment of the electron and hole as independent particles, we now need to consider their interaction. In an isoelectronic model, the ground state of the system is the ''vacuum'' state with no particles. It therefore has a spin of $S=0$, and optical transitions are only allowed to it from the singlet excited states. Line C is not perturbed by the magnetic fields and so has an $S=0$ excited state. It also has a relatively high transition probability [Eq. (1)]. The excited state of line C can be conveniently labeled $^1T_2$ in a T_d notation. If the spins of the electron and hole can combine to give $S=0$, then $S=1$ combinations are also expected. Line A splits isotropically into five components in a magnetic field (Fig. 3). Borrowing atomic physics notation, a T_2 state has orbital angular momentum $l=1$, which combines with $S=1$ to give $J=2$, 1, and 0; the $J=2$ state would split into five components in a magnetic field, as does line A. Using a spin-orbit coupling $H_{so}=\lambda \mathbf{L}\cdot\mathbf{S}$ and assigning the triplet state to line B predicts the $J=0$ state 0.3 meV above B. This state can be observed in luminescence when it is induced by ⟨110⟩ uniaxial stresses, Fig. 5. The same splittings are observed for the 796-meV group of lines (Fig. 4), and here the line ascribed to $J=0$ can be observed at zero field at 797.2 meV. As required, it is not split by the magnetic field. The lines near 796 meV could therefore originate from the same electronic states as lines A, B, and C, with a hole state 16.9 meV higher than that involved in those lines.

For a more detailed description, it is convenient to write the $^3T_2$ states in the angular momentum form

$$|1\rangle=(T_2^x+iT_2^y)/\sqrt{2},\quad |0\rangle=T_2^z,\quad |-1\rangle=(T_2^x-iT_2^y)/\sqrt{2}.$$

The perturbation caused by the magnetic field is

$$\Delta H_z=\mu_B(g_L\mathbf{L}+g_S\mathbf{S})\cdot\mathbf{B}. \tag{3}$$

The combined stress and Zeeman perturbation matrix for the spin triplet states is given in the Appendix. The best fit to the Zeeman data for lines A and B gives $\lambda=-0.46$ meV, $g_S=1.9\pm0.1$, and $g_L=0$ (Fig. 3). Transitions induced from line F_0, shown by the diamonds in Fig. 3, are described well by simply downshifting the fits to the lowest-energy components of line A. The value $g_L=0$ is as required for valley-orbit states. The same scheme also fits the overall splitting of the lines near 797 meV, with the same parameters $\lambda=-0.46$ meV and $g_L=0$, but with a slightly reduced $g_S=1.3\pm0.1$, Fig. 4.

To fit the stress data requires the inclusion of the hole state, moving in trigonal symmetry, with the C_{3v} point group. To define the notation we consider a particular orientation of the C_{3v} optical center with the C_3 axis parallel to [111] and with one of the reflection planes perpendicular to $[1\bar{1}0]$. The hole is perturbed as

$$\Delta V_h=a_1(s_{xx}+s_{yy}+s_{zz})+a_2(s_{yz}+s_{zx}+s_{xy}), \tag{4}$$

where the a_i are electronic operators.[23] Only two parameters A_1 and A_2 are required to describe the effect of stresses on the hole state, corresponding to the effect of each of the operators a_1 and a_2 of Eq. (4). From an optical transition we only measure the *difference* in energy between states. Consequently, we can measure the difference in their perturbations by totally symmetric stresses, but not the absolute perturbations. We therefore absorb the perturbation by hydrostatic stresses of the electron state into that of the hole state. The best fit to the effect of uniaxial stresses on the transitions A, B, and C is shown by the lines in Fig. 5. For the singlet states, the T_2 level is perturbed as in Eq. (2). The perturbations of the optical transitions have been defined as the difference between the electron energies and the hole energies, and the compressive stress is positive. With these conventions, the best-fitting values are, with $\pm15\%$ uncertainty, $A_1=6.5$ meV/GPa and $A_2=3.7$ meV/GPa. The one parameter for the electron state is $C=-11.2\pm1.5$ meV/GPa. This value is very similar to that of -11 meV/GPa found at the well-known 789-meV carbon-oxygen center[24] and is comparable to the free-electron parameter of -15.4 meV/GPa.[21]

We have noted the close similarity in the zero-field splitting and magnetic field perturbations of the multiplet near 796 meV and lines A, B, and C. The stress data for these lines can also be fitted using the same stress parameters as for A, B, and C, Fig. 6. Similarly, the higher-energy multiplet

near 820 meV splits with the same shift rates as the corresponding components of line *C* (Fig. 6).

The model presented here describes a considerable amount of perturbation data using an electron state derived from the T_2 valley-orbit states. The excited state of the line F_0 does not form part of this scheme. We have not been able to determine the nature of that state since the F_0 line is so weak. However, we note that the *E* valley-orbit states may be expected to be of a similar energy to the T_2 states, and they *could* form the electron component of the exciton. The degeneracy g_F of the triplet *E* state would then be $g_F=6$; its exact value is not critical in its use below in Sec. VII.

V. ELECTRON-PHONON COUPLING

The phonon sidebands F_1 and F_2 are associated with a forbidden zero-phonon line F_0, Sec. III. This situation arises when a vibration of the optical center couples the electronic state from which transitions are forbidden to one from which optical transitions are allowed. The simplest case is when the Hamiltonian of the center contains a term that is linear in the displacement of the relevant vibrational mode. The molecular deformation produced by a vibration is expected to perturb the orbital parts of the states rather than their spins and so will only couple states of the same spin. The line F_0 is not readily detectable, but magnetic fields induce and shift the lower-energy components as for line *A* (Fig. 3), suggesting that the excited state of F_0 is effectively another quintuplet. However, a definite assignment cannot be made to F_0 since we do not see a full Zeeman splitting, and so we will allow F_0 to interact with the excited states of either *A* or *B*. However, we can exclude coupling of F_0 with the spin-singlet excited state of line *C*. The vibrational modes will be represented by one effective vibrational mode (with quantum energy of $\hbar\omega$). In the absence of the vibronic coupling, the states can be represented by Born-Oppenheimer products of the *electronic states* $\phi_X(r)$ $(X=F,A,B)$ and the harmonic vibrational states $\chi_i(Q)$:

$$\psi_{Xi}=\phi_X(r)\chi_i(Q), \tag{5}$$

where *r* represents the coordinates of the electrons, *Q* is the vibrational coordinate, and $i=1,2,...,\infty$ indicates the vibrational state. These states are coupled by an electron-phonon term $\hat{d}Q$ that is linear in the mode displacement *Q*, where $\hat{d}$ is an electronic operator. We define the strengths of these interactions as

$$c_1=\langle\phi_A|\hat{d}|\phi_F\rangle=\langle\phi_F|\hat{d}|\phi_A\rangle, \tag{6a}$$

$$c_2=\langle\phi_B|\hat{d}|\phi_F\rangle=\langle\phi_F|\hat{d}|\phi_B\rangle. \tag{6b}$$

Since there are negligible phonon sidebands originating from zero-phonon lines *A* and *B*, the effect of $\hat{d}Q$ on the states ϕ_A and ϕ_B themselves is approximately zero:

$$\langle\phi_A|\hat{d}|\phi_A\rangle=\langle\phi_B|\hat{d}|\phi_B\rangle=0. \tag{7}$$

Similarly, we have no evidence for any phonon sidebands occurring through simple relaxation of the state *F*, and so

$$d=\langle\phi_F|\hat{d}\rangle|\phi_F=0. \tag{8}$$

The state ψ_{Fi} is mixed with ψ_{Aj} and ψ_{Bk} by the coupling, producing new eigenstates Ψ_{Fp}, Ψ_{Aq}, and Ψ_{Br}, which lie in the space spanned by ψ_{Fi}, ψ_{Aj}, and ψ_{Bk}:

$$\Psi_{Xp}=\sum_i f_{Xpi}\psi_{Fi}+\sum_j a_{X_{pj}}\psi_{Aj}+\sum_k b_{X_{pk}}\psi_{Bk}. \tag{9}$$

The coefficients f_{Xpi}, a_{Xpj}, and b_{Xpk} may be found from the secular matrix, which has a very simple form. For each state $X=F$, *A*, and *B* with the same vibrational quantum state *p*,

$$\langle\psi_{Xp}|H|\psi_{Xp}\rangle=E_X^0+(\tfrac{1}{2}+p)\hbar\omega, \quad p=0,1,2,..., \tag{10}$$

where *H* is the Hamiltonian, including the vibronic coupling, and E_X^0 is the energy of the (uncoupled) electronic state *X*. All the other elements of the matrix are zero except where those pairs of states are coupled by $\hat{d}Q$. The effect of $\hat{d}$ on the electronic part of the Born-Oppenheimer products is defined by Eqs. (6) and (7). Since the coupling term $\hat{d}Q$ is linear in *Q*, it only couples vibrational states that differ by ±1 in the quantum number. The coupling therefore has the form

$$\begin{aligned}\langle\psi_{Fi}|\hat{d}Q|\psi_{Aj}\rangle&=\langle\phi_F|\hat{d}|\phi_A\rangle\langle\chi_i|Q|\chi_{i\pm1}\rangle\\&=c_1\sqrt{\frac{\hbar}{2m\omega}}\sqrt{i+1}\,\delta_{j,i+1}\\&\quad+c_1\sqrt{\frac{\hbar}{2m\omega}}\sqrt{i}\,\delta_{j,i-1},\end{aligned} \tag{11}$$

with corresponding expressions for the coupling of ψ_{Fi} to ψ_{Bj}.

The eigenvalues and eigenvectors of the secular matrix can be found numerically. The variable parameters in the matrix are the differences between the three energies of the electronic states E_X^0 without vibronic coupling, the coupling $c_1/\sqrt{m\omega}$ between states *F* and *A*, and the coupling $c_2/\sqrt{m\omega}$ between *F* and *B*. The measured data are the energies of the zero-phonon states, $E_F=778.6$ meV, $E_A=778.9$ meV, and $E_B=779.85$ meV, the quantum $\hbar\omega$ (which we set equal to the quantum of the mode of $\hbar\omega=5.8$ meV, since it is seen most strongly in the spectra), and the relative transition probabilities of line *A* to line F_1 and *A* to *B*; we may also set the transition probability for the zero-phonon line F_0 equal to zero. The energy levels of the lowest vibronic states are shown in Fig. 7 as a function of the coupling term $c_1\sqrt{\hbar/2m\omega}$.

It is found that a good fit can only be obtained when F_0 couples predominantly with *either* state *A or* state *B*. The coupling is to the state *A* since the two-phonon line at 767.2 meV is observable as a result of the vibronic coupling, and its energy—and also the fact that it can be observed at temperatures when the zero-phonon line *B* is very weak (Fig. 1)—implies that it is produced by the *A* state. A least-squares fit to the data then gives

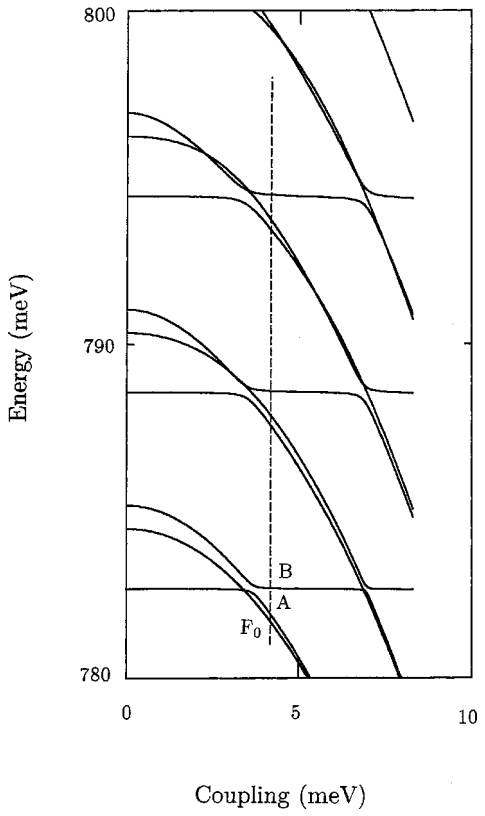

FIG. 7. The energies of the lowest vibronic levels of the electronic states *F, A,* and *B* as a function of the coupling $c_1\sqrt{\hbar/2m\omega}$, calculated with $c_2/c_1=0.06$. The phonon energy has been taken as 5.8 meV. The vertical dashed line shows the value of the coupling that gives the best fit to the energy separations of F_0, *A,* and *B*. The resulting predicted spectrum is shown by the simulated spectrum at the bottom of Fig. 1. The ground vibronic states are assumed to involve harmonic vibrations of the same 5.8-meV quantum.

$$c_1\sqrt{\hbar/2m\omega}=4.2\ \text{meV}, \quad c_2/c_1=0.06, \tag{12}$$

and the energies of *F, A,* and *B* in the absence of vibronic coupling are obtained as $E_F^0=781.5$ meV, $E_A^0=782.2$ meV, and $E_B^0=779.7$ meV.

The photoluminescence band shape, calculated for $T=4.2$ K, is shown in Fig. 1. It is very similar to the measured spectrum with the exception that the line F_2 is omitted, since our model uses only one mode. The coupling produces a strong one-phonon transition F_1 associated with the zero-phonon line F_0, but one-phonon transitions from both *A* and *B* are forbidden. The weak coupling between the states *F* and *B* leads to undetectable two-phonon transitions from the *B* state. The calculation shows that the phonon line at 767.2 meV (A_1^2) reported as a local mode with energy of 12 meV,[15] in fact, is produced by a two-phonon transition involving the 5.8-meV mode and occurs as a consequence of the electron-phonon coupling between states *A* and *F*.

In this section we have seen that the luminescence band shape is unusual in that the phonon sidebands are not linked directly to the dominant zero-phonon lines. This type of vibronic coupling appears to have been reported for only one other point defect in silicon.[25] We have shown that the spectral shape is produced by a vibronic interaction between the lowest observed state F_0 and the next observed state *A*. Confirmation of the model would be provided by an independent assessment of c_1. From Eq. (12), evaluation of c_1 requires knowledge of the effective mass *m* of the vibration. This information is provided by isotope doping.

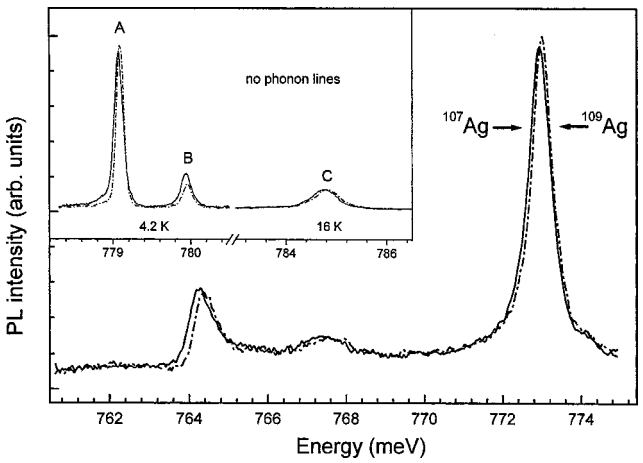

FIG. 8. Photoluminescence spectra recorded from samples doped with single isotopes of ^{107}Ag or ^{109}Ag. The main figure shows the effects on the one-phonon lines F_1, A_1^2, and F_2. The inset shows the effect on the lines *A, B,* and *C,* in agreement with Ref. 20.

VI. ISOTOPE EFFECTS

Henry *et al.*[26] have shown that doping with Ag can result in optical centers formed from accidental impurities. Figure 8 shows the effect of doping with single isotopes of Ag, rather than with natural silver, which has an isotopic composition of ^{107}Ag:^{109}Ag=52:48. Both the zero-phonon lines and one-phonon sidebands are observed at higher energy in ^{109}Ag than in ^{107}Ag, with the energy separation of *A* and F_1 decreasing by 0.09 ± 0.01 meV and that of *A* and F_2 decreasing by 0.16 ± 0.1 meV. The zero-phonon shifts could be caused by different lattice strains, but taken together with the significantly greater one-phonon shifts, the data unambiguously demonstrate the presence of at least one Ag atom in the optical center.

With natural Ag, the modes that produce the bands F_1 and F_2 have well-defined quanta of $E_1=5.8$ meV and $E_2=14.6$ meV (Sec. III). If we assume that the zero-phonon level F_0 changes with isotopes in the same way as the closely adjacent line *A*, then the fractional changes in phonon energies are $\Delta F_1\sim-0.012$ and $\Delta F_2\sim-0.01$ from ^{107}Ag to ^{109}Ag. A very simple model of a heavy ion vibrating in a lattice shows that the frequency of vibration is approximately inversely proportional to the mass difference ΔM of the heavy (Ag) ion and the host lattice (Si) (Ref. 27); this model provides a qualitative understanding of the resonance modes of heavy ions in diamond.[28] Applied to ^{107}Ag and ^{109}Ag in ^{28}Si, it gives a fractional shift of -0.012, consistent with the observed changes.

The appropriate mass to use in evaluating c_1 is therefore that of the Ag atom. Then,

$$c_1 = 1.1 \times 10^{-10} \text{ J/m}. \tag{13}$$

Converting c_1 to strain,

$$c_1' = b c_1 = 0.2 \text{ eV/strain}, \tag{14}$$

where b is the interatomic spacing of the Si crystal (0.234 nm). Strain parameters in silicon are typically of the order of 1 eV/strain, confirming that c_1 has a sensible order of magnitude. The line F_0 is induced by stresses applied along the $\langle 111 \rangle$ and $\langle 110 \rangle$ directions, but not the $\langle 001 \rangle$ direction, Fig. 5. This suggests that the shear stresses $s_{yz}+s_{zx}+s_{xy}$ of Eq. (4) couple F_0 to A. The coupling cannot, in practice, be determined from the data in Fig. 3. However, the value of the shear parameter $A_2 = 3.7$ meV/GPa corresponds to a strain parameter of $c_{44}A_2 = 0.3$ eV/strain, again of a similar magnitude to c_1'.

VII. THERMAL QUENCHING OF THE LUMINESCENCE

Figure 9 shows, as functions of temperature, the luminescence intensity integrated across all the band (triangles) and the radiative decay times of lines A (squares) and B (crosses), measured in independent samples. As the temperature increases to ~35 K, the total intensity increases with the increasing population of state C, from which transitions are strongly allowed (Sec. III). The decrease at high temperature occurs generally for luminescence centers in silicon, Sec. I. We know from Sec. III that all the excited states of the center reach thermal equilibrium before the photoluminescence transition occurs and so the intensity is expected to follow

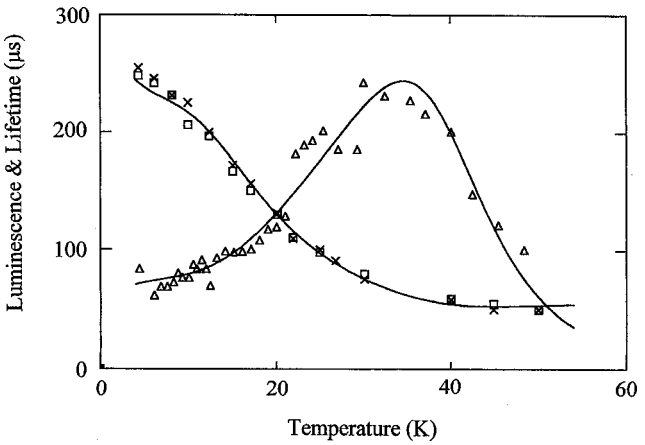

FIG. 9. The intensity (arbitrary units) of the total luminescence from the band as a function of temperature is shown by the triangles. The temperature dependences of the measured radiative decay times of lines A and B are shown by the squares and crosses, respectively. The lines are the least-squares fit of Eqs. (15) and (16).

$$I(T) \approx \frac{I(0)[1+\Sigma_i(\tau_F g_i/\tau_i g_F)\exp(-E_i/kT)]}{1+\Sigma_i(g_i/g_F)\exp(-E_i/kT)+(g/g_F)T_{3/2}\exp(-E_a/kT)}. \tag{15}$$

Here the sums are over all the states $i=A$, B, and C and $1/\tau_i$ is the mean transition probability for the radiative transitions originating each of the g_i degenerate states of the state at an energy E_i above F_0. The thermal quenching of the excited states has an activation energy E_a and an effective degeneracy of $(g/g_F)T^{3/2}$ relative to state F_0.

The decay times as measured for lines A and B from 4 to 50 K are also shown in Fig. 9. Lines A, B, and C decay exponentially with time after a pulse of excitation. Since their excited states are in thermal equilibrium, Sec. III, their decay times are equal at each temperature. Corresponding to Eq. (15), the decay time τ is given by

$$\frac{1}{\tau(T)} = \left(\frac{g_F}{\tau_F}\right)\left[\frac{1+\Sigma_i(\tau_F g_i/\tau_i g_F)\exp(-E_i/kT)+(r_g/g_F)T^{3/2}\exp(-E_a/kT)}{1+\Sigma_i(g_i/g_F)\exp(-E_i/kT)+(g/g_F)T^{3/2}\exp(-E_a/kT)}\right]. \tag{16}$$

Here the term r determines the rate of ionization into the continuum.

In Eqs. (15) and (16), the values of E_i are known from the optical spectra, and $g_F=6$, $g_A=5$, $g_B=3$, and $g_C=1$, from Secs. IV and V. From the measured ratio of the probabilities of transitions F, A, and B, Eq. (1), we know the ratios τ_F/τ_A and τ_B/τ_A: $\tau_F/\tau_A = (I_A g_F/I_F g_A) = 1.8$ and $\tau_B/\tau_A = (I_A g_B/I_B g_A) = 0.9$. The thermal-quenching energy E_a is best found from the luminescence data. It is not sensitive to the other parameters, and a least-squares fit gives $E_a = 33.3 \pm 1$ meV. This value is in agreement with the threshold of photoionization from the excited states [$E_a = 33$ meV (Ref. 29)]. It is also comparable to the value of 41.7 meV for the binding energy relative to state C, derived indirectly by assuming that the transition at 816 meV involves an effective-mass electron in a $2p_0$ state, which can be compared to the energy levels of a donor.[17] The value of E_a has been fixed at 33.3 meV. A least-squares fit of Eqs. (15) and (16) to all the data in Fig. 9 can now be made with five adjustable parameters. They are determined as $\tau_A = 1020$ μs, $\tau_C = 6.3$ μs, $g = 490$ K$^{-3/2}$, and $r = 435$, plus the physically insignificant $I(0) = 60$. Variations in the fitting strategy can change τ_A and r by 50%, while τ_C and g appear to be stable to $\pm 10\%$. Radiative decay times in the microsecond range are typical for centers in silicon with diffuse excited states. From the parameters, we have $I_F/I_C = (g_F\tau_C)/(g_C\tau_F) = 0.02 \pm 0.01$, confirming the value in Eq. (1).

TABLE I. The effects of stress and magnetic fields on a T_2 state coupled to spin 1.

$H_{so}+V$	$\|1\rangle\|1\rangle$	$\|1\rangle\|0\rangle$	$\|1\rangle\|-1\rangle$	$\|0\rangle\|1\rangle$	$\|0\rangle\|0\rangle$	$\|0\rangle\|-1\rangle$	$\|-1\rangle\|1\rangle$	$\|-1\rangle\|0\rangle$	$\|-1\rangle\|-1\rangle$
$\|1\rangle\|1\rangle$	$z+z'$ $+\lambda-Cs_\theta$	$-\frac{1}{\sqrt{2}}(x+iy)$	$\sqrt{3}Cs_\epsilon$	$\frac{1}{\sqrt{2}}(x'+iy')$	0	0	0	0	0
$\|1\rangle\|0\rangle$		$z'+2Cs_\theta$	$\frac{1}{\sqrt{2}}(x+iy)$	λ	$\frac{1}{\sqrt{2}}(x'+iy')$	0	0	0	0
$\|1\rangle\|-1\rangle$			$z'-z$ $-\lambda-Cs_\theta$	0	λ	$\frac{1}{\sqrt{2}}(x'+iy')$	0	0	0
$\|0\rangle\|1\rangle$				$z-Cs_\theta$	$-\frac{1}{\sqrt{2}}(x+iy)$	$\sqrt{3}Cs_\epsilon$	$\frac{1}{\sqrt{2}}(x'+iy')$	0	0
$\|0\rangle\|0\rangle$					$2Cs_\theta$	$\frac{1}{\sqrt{2}}(x+iy)$	λ	$\frac{1}{\sqrt{2}}(x'+iy')$	0
$\|0\rangle\|-1\rangle$						$-z-Cs_\theta$	0	λ	$\frac{1}{\sqrt{2}}(x'+iy')$
$\|-1\rangle\|1\rangle$							$z-z'$ $-\lambda-Cs_\theta$	$-\frac{1}{\sqrt{2}}(x+iy)$	$\sqrt{3}Cs_\epsilon$
$\|-1\rangle\|0\rangle$								$-z'+2Cs_\theta$	$\frac{1}{\sqrt{2}}(x+iy)$
$\|-1\rangle\|-1\rangle$									$-z-z'$ $+\lambda-Cs_\theta$

We can now clarify why in our fitting procedure we first obtained the quenching energy E from the luminescence intensity. If there was no quenching, the luminescence would increase and saturate as state C became populated. The quenching therefore has a major effect on the total luminescence. In contrast, it has a smaller absolute effect on the lifetime, which is already severely reduced by the relatively short lifetime of the excited state of line C. By combining the data, we can estimate the rate of thermal ionization, which does not appear to have been presented for any pseudodonor in silicon. In Eq. (16) the term $(r_g/\tau_F)T^{3/2}\exp(-E_a/kT)$ represents the thermally activated quenching of the luminescence, which consists of a Boltzmann term and the usual preexponential, which is temperature dependent. At 50 K, the prefactor has the value 4×10^{10} Hz, surprisingly slower than the frequency ($\sim10^{12}$ Hz) of the dominant 5.8-meV phonon.

VIII. SUMMARY

We have reported the results of a detailed phenomenological study of the optical properties of a silver-related center in silicon. Perturbations of the optical transitions by uniaxial stresses and magnetic fields have been accurately described in terms of an effective-mass electron, orbiting the center in a triply degenerate orbital state in effectively T_d symmetry, and a tightly bound hole, which has its angular momentum quenched by the local trigonal field of the center (Sec. IV). These particles couple through their spin. At a slightly lower energy than these readily observed states, a state exists from which optical transitions are strongly forbidden, but which is phonon-coupled to the other electronic states. As a result, the vibronic sidebands observed at low temperature derive from the forbidden zero-phonon line (Sec. V). Using an effective mass for the vibrational mode derived from isotope data (Sec. VI), we have shown that the required magnitude of the electron-phonon coupling is of a reasonable magnitude. With this energy-level scheme, the total luminescence and the radiative decay time have been fitted over the temperature range 4–50 K, and it has been shown that the data can give an estimate of the time taken to thermally ionize an electron from an effective-mass state (Sec. VII). A highly detailed phenomenological understanding of the optical properties can therefore be achieved, even though the molecular structure of the core of the center has not been determined.

ACKNOWLEDGMENTS

M.Z. thanks the Overseas Research Student Award Scheme, the K C Wong Education Foundation, and The Henry Lester Trust Ltd. for financial support. M.Z.I. thanks the Commission of European Communities for the support as a visiting scientist to Kings College London. This work was supported by the Engineering and Physical Sciences Research Council.

APPENDIX

Table I gives the effect of stress and magnetic fields on a T_2 state coupled to a spin of 1. The matrix is ordered as

$|\text{spin}\rangle|\text{orbital}\rangle$, with the orbital parts defined in Sec. III. Terms in the lower section of the matrix are given by the complex conjugates of the corresponding terms in the upper part.

For brevity, in Table I, $x=\mu_B g_x B_x$, $y=\mu_B g_y B_y$, $z=\mu_B g_z B_z$, $x'=\mu_B g_s B_x$, $y'=\mu_B g_s B_y$, $z'=\mu_B g_s B_z$. Here the components of the field are B_x, B_y, and B_z, μ_B is the Bohr magneton, g_s is the spin g factor, and the components of the orbital g factor are g_x, g_y, and g_z.

*Deceased.

[1] J. Weber, H. Bauch, and R. Sauer, Phys. Rev. B **25**, 7688 (1982).

[2] T. G. Hall and D. G. Brown, Appl. Phys. Lett. **49**, 245 (1986).

[3] K. Thonke, J. Weber, J. Wagner, and R. Sauer, Physica B **116**, 252 (1983).

[4] G. Davies, Phys. Rep. **176**, 83 (1989).

[5] A. N. Safonov, E. C. Lightowlers, G. Davies, P. Leary, R. Jones, and S. Öberg, Phys. Rev. Lett. **77**, 4812 (1996).

[6] G. Davies, Phys. Scr. **T54**, 7 (1994).

[7] G. Davies, Phys. Rev. B **51**, 13 783 (1995).

[8] N. Baber, H. G. Grimmeiss, M. Kleverman, P. Omling, and M. Z. Iqbal, J. Appl. Phys. **62**, 2853 (1987).

[9] N. T. Son, V. E. Kustov, T. Gregorkiewicz, and C. A. J. Ammerlaan, Phys. Rev. B **46**, 4544 (1992).

[10] N. T. Son, T. Gregorkiewicz, and C. A. J. Ammerlaan, J. Appl. Phys. **73**, 1797 (1993).

[11] J. Olajos, M. Kleverman, and G. Grimmeiss, Phys. Rev. B **38**, 10 633 (1988).

[12] M. Kleverman, J. Olajos, G. Grossmann, B. Bech-Nielsen, and H. G. Grimmeiss, Phys. Scr. **T25**, 134 (1989).

[13] J. H. Svensson, B. Monemar, and E. Janzén, Phys. Rev. Lett. **65**, 1796 (1990).

[14] M. Z. Iqbal, G. Davies, and E. C. Lightowlers, Mater. Sci. Forum **143–147**, 773 (1994).

[15] N. T. Son, M. Singh, J. Dalfors, B. Monemar, and E. Janzén, Phys. Rev. B **49**, 17 428 (1994).

[16] I. De Maat-Gersdorf, T. Gregorkiewicz, and C. A. J. Ammerlaan, J. Lumin. **60–61**, 556 (1994).

[17] M. Singh, W. M. Chen, B. Monemar, and E. Janzén, Solid State Commun. **93**, 415 (1995).

[18] M. Zhu, G. Davies, M. Z. Iqbal, and E. C. Lightowlers, Mater. Sci. Forum **258–263**, 485 (1997).

[19] N. Q. Vinh, M. A. J. Klik, and T. Gregoriewicz, Physica B **308–310**, 414 (2001).

[20] N. Q. Vinh, T. Gregorkiewicz, and K. Thonke, Phys. Rev. B **65**, 033202 (2001).

[21] L. D. Laude, F. H. Pollack, and M. Cardona, Phys. Rev. B **3**, 2623 (1971).

[22] D. K. Wilson and F. Feher, Phys. Rev. **124**, 1068 (1961).

[23] A. A. Kaplyanskii, Opt. Spectrosc. **16**, 329 (1964).

[24] K. Thonke, A. Hangleiter, J. Wagner, and R. Sauer, J. Phys. C **18**, L795 (1985).

[25] G. Davies and M. C. do Carmo, in *Shallow Impurities in Semiconductors, Proceedings of the 3rd International Conference, Linköping, Sweden, 1988*, Inst. Phys. Conf. Ser. No. 95, edited by B. Monemar (IOP, Bristol, 1989), p. 125.

[26] M. O. Henry, S. E. Daly, C. A. Frehill, E. McGlynn, C. McDonagh, E. Alves, J. C. Soares, and D. Forkel, in *Proceedings of the 23rd International Conference on the Physics of Semiconductors* (World Scientific, Singapore, 1996), p. 2713.

[27] R. Brout and W. Visscher, Phys. Rev. Lett. **9**, 54 (1962).

[28] A. M. Zaitsev, Phys. Rev. B **61**, 12 909 (2000).

[29] Q. N. Vinh, in MRS Spring Meeting 2003 (Materials Research Society, Pittsburgh, to be published).